논문 01-02-05

Dynamic Electrical Impedance Tomography with Internal Electrodes

내부 전극을 이용한 동적 전기 임피던스 단층촬영법

Suk-In Kang*, Kyung-Youn Kim**
(姜 淑 仁* , 金 慶 淵**)

Abstract

Electrical impedance tomography(EIT) is a relatively new imaging modality in which the internal impedivity distribution is reconstructed based on the known sets of injected currents and measured voltages on the surface of the object. We describe a dynamic EIT imaging technique for the case where the resistivity distribution inside the object changes rapidly within the time taken to acquire a full set of independent measurement data. In doing so, the inverse problem is treated as the state estimation problem and the unknown state (resistivity) is estimated with the aid of extended Kalman filter in a minimum mean square error sense. In particular, additional electrodes are attached to the known internal structure of the object to enhance the reconstruction performance and modified Tikhonov regularization technique is employed to mitigate the ill-posedness of the inverse problem. Computer simulations are provided to illustrate the reconstruction performance of the proposed algorithm.

요 약

전기 임피던스 단층촬영법은 물체 표면의 전극을 통하여 전류를 주입하고 유기된 전압을 측정한 후, 물체 단면의 저항율 분포를 복원하는 기법이다. 본 논문에서는, 대상물체의 저항율 값의 분포가 급변하는 상황에 대한 동적 전기저항 단층촬영법을 제안하였다. 특히, 복원 성능을 개선하기 위하여 물체 내부의 구조를 전극으로 사용하였으며, 비 선형 역문제를 상태 추정문제로 설정하여 확장 칼만필터를 이용하여 상태변수(저항율)를 추정하였다. 또한 역문제의 부정치성을 완화시키기 위하여 수정된 Tikhonov 조정기법을 비용함수에 도입하였다. 제안된 알고리즘의 성능을 분석하기 위해 컴퓨터 시뮬레이션을 수행했으며, 기존의 방법들에 비해 개선된 결과를 얻었다.

Key words: Dynamic EIT, internal electrodes, state estimation, extended Kalman filter,Tikhonov regularization

I. Introduction

Over the past few decades, Electrical Tomography (ET) techniques have received much attention from both theoretical and experimental points of view since they can be used as an alternative imaging modality for monitoring tool in many fields of engineering. This is mainly due to the relatively cheap electronic hardware requirements, noninvasive measurement sensing, and relatively good temporal resolution [1-7].

* 濟州大學校 電氣電子工學部
(Department of Electrical & Electronic Engineering, Cheju National University)
接受日: 2001年 8月 1日, 修正完了日: 2001年11月10日

If the electromagnetic properties of different materials inside the object differs from each other the spatial and/or temporal distributions of the material properties can be estimated based on the various ET techniques. In general, the ET techniques can be classified into three categories according to the electromagnetic quantities to be imaged; These quantities are the magnetic permeability(μ), electric permittivity(ε), and electric conductivity(σ), which correspond to Electro-Magnetic Inductance Tomography (EMIT)[8], Electrical Capacitance Tomography (ECT)[9] and Electrical Resistance Tomography (ERT)[10], respectively. In all of the above tomographic techniques, the relationships between the electromagnetic quantities inside the object and sensing quantities on the surface are described by the Maxwells equations [1].

In Electrical Impedance Tomography(EIT), the quantity to be imaged is actually the impedivity (inverse of admittivity) so that it includes both ECT and ERT. However, more frequently in EIT it assumed that the resistive part of the impedivity dominates and estimate only the resistivity (inverse of conductivity) distribution inside the object. The physical relationship between the internal resistivity and the surface voltages is governed by a partial differential equation (Laplace equation) with appropriate boundary conditions. Owing to the complexity of this relationship, it is in most cases impossible to obtain a closed-form solution for the resistivity distribution. Hence, various reconstruction algorithms have been developed in the literature to estimate the internal resistivity distribution of the object.

However, most of the reconstruction algorithms presented so far are mainly focused on the case where the internal resistivity of the object is time-invariant within the time taken to acquire a full set of independent measurement data. As is well known, the conventional EIT imaging techniques such as backprojection or modified Newton-Raphson (mNR) algorithm use a full set of voltage measurements for each image [11,12]. However, in some real applications such as biomedical and chemical processes, these static imaging techniques are often fail to obtain satisfactory temporal resolution for the reconstructed images due to the rapid changes in resistivity.

More recently, dynamic imaging techniques have been developed to enhance the temporal resolution of the reconstructed images in the situations where the resistivity distribution inside the object changes rapidly in time. In most of these techniques, the inverse reconstruction problem is treated as state estimation problem and the time-varying state is estimated with the aid of linearized Kalman filter (LKF)[13-17] or extended Kalman filter (EKF)[18, 19].

Quite often in real situations there are partially known fixed internal structures inside the object. These internal structures can be, for example, an impeller drive shaft or a mixing paddle in process vessels and an assembly of fuel rods in nuclear reactor. The internal structures inside the object may results in difficulties in the image reconstruction in EIT especially in the case where the high resistive region is near the conductive internal structure or vice versa[20, 21]. The so-called masking effect in the reconstructed image may be significant for the high-contrast case. There are two ways to get around these difficulties; the one is to use the internal structure as additional electrodes [20, 22, 23] and the other is to take into account it as a priori information in the inverse procedure [21]. However, all of the above approaches are for the case where the resistivity distribution inside the object is time-invariant for one classical frame.

The purpose of the present work is to develop a dynamic EIT reconstruction algorithm for the case where the fixed internal structures are known partially and the resistivity distribution of the other part inside the object changes rapidly within the time taken to acquire a full set of independent measurement data. To achieve the purpose, additional electrodes are attached to the known internal structure. The inverse problem is treated as the state estimation problem and the unknown state (resistivity) is estimated with the aid of the EKF in a minimum mean square error sense. In other to deal with the well-known ill-posedness of the EIT inverse problem, smoothness assumption is made and the modified Tikhonov regularization technique is also introduced in the cost functional.

We carried out extensive computer simulations with

synthetic data to illustrate the reconstruction performance, and to investigate the effects of additional internal electrodes on the spatial and temporal resolution of the reconstructed images.

The rest of the paper is organized as follows. In Section II, we formulate the EIT forward problem based on the complete electrode model (CEM)[16, 24] and describe the numerical solver by the finite element method (FEM). The inverse solver based on the EKF is presented in Section III, where the inverse problem is treated as state estimation problem in a minimum mean square error sense. Extensive computer simulation results are given in Section IV. Here, special attention is given to the effects of additional internal electrodes on the spatial and temporal reconstruction performance. Concluding remarks are given in the final Section.

II. Formulation of the Problem and Forward Solver

When electrical currents Il (l=1,2,...,L) are injected into the object $\Omega \in R2$ through the electrodes el (l=1,2,...,L) attached on the boundary $\partial\Omega$ and the resistivity distribution $\rho(x,y)$ is known for the Ω, the corresponding electrical potential u(x,y) on the Ω can be determined uniquely from the partial differential equation, which can be derived from the Maxwell equations:

$$\nabla \cdot \left(\frac{1}{\rho} \nabla u\right) = 0 \quad in \ \Omega \tag{1}$$

with the following boundary conditions based on the complete electrode model :

$$u + z_l \frac{1}{\rho} \frac{\partial u}{\partial n} = U_l, \qquad x \in e_l, \ l = 1,2,\ldots,L \tag{2-a}$$

$$\int_{e_l} \frac{1}{\rho} \frac{\partial u}{\partial n} dS = I_l \qquad x \in e_l, \ l = 1,2,\ldots,L \tag{2-b}$$

$$\frac{1}{\rho} \frac{\partial u}{\partial n} = 0 \ , on \ \ \partial\Omega \setminus \bigcup_{l=1}^{L} e_l \tag{2-c}$$

where, zl is the effective contact impedance between lth electrode and electrolyte, Ul is the potential on the lth electrode, el is lth electrode, n is outward unit normal, and L is number of electrodes. Despite different form of the boundary conditions may be used in the forward model, we choose the CEM which takes into account the discrete electrodes, effects of the contact impedance, and the shunting effect of the electrodes.

In addition, the following two constraints for the injected currents and measured voltages are needed to ensure the existence and uniqueness of the solution:

$$\sum_{l=1}^{L} I_l = 0 \tag{3-a}$$

$$\sum_{l=1}^{L} U_l = 0 \tag{3-b}$$

The computation of the potential u(x,y) on the Ω and the voltages Ul on the electrodes for the given resistivity distribution $\rho(x,y)$ and boundary conditions is called the forward problem. In general, the forward problem can not be solved analytically we have to resort to the numerical method. There are different numerical methods such as the finite difference method (FDM), boundary element method(BEM), and finite element method (FEM). In this paper, we used the FEM to obtain numerical solution. In FEM, the object area is discretized into sufficiently small elements having a node at each corner and it is assumed that the resistivity distribution is constant within each element. The potential at each node and the "referenced" electrode voltages, defined by the vector $v \in R^{M+L-1}$, are calculated by discretizing (1) into $Yv = c$, where $Y \in R^{(M+L-1)\times(M+L-1)}$ is so-called stiffness matrix and M is the number of FEM nodes. Y and c are the functions of the resistivity distribution in the object and the injected currents through the electrodes, respectively. For more details on the forward solution and the FEM approach, see [16, 25].

III. Inverse Solver Based on the Extended Kalman Filter

In case where the resistivity distribution inside the object changes rapidly within the time taken to acquire a full set of independent measurement data, the conventional imaging techniques which need a full set of voltage measurements for each image often fail to obtain satisfactory temporal information on the resistivity distribution. We consider the underlying inverse problem as a state estimation problem to estimate rapidly time-varying distribution of the resistivity. In the state estimation problem, we need so-called the dynamic model which consists of the state equation, i.e., for the temporal evolution of the resistivity and the observation equation, i.e., for the relationship between the resistivity and boundary voltage.

In general, the temporal evolution of the resistivity distribution ρ_k in the object Ω is related by the nonlinear mapping. Here, the state equation is assumed to be of the linear form, of which the modeling uncertainty is compensated by the process noise

$$\rho_{k+1} = F_k \rho_k + w_k \tag{4}$$

where $F_k \in$ RN×N is the state transition matrix at time k and N is the number of finite elements in the FEM. In particular, we take $F_k \equiv I_N$ where $I_N \in$ RN×N is an identity matrix, to obtain the so-called random-walk model. It is assumed that the process error, wk is white Gaussian noise with the following covariance which determines the rate of changes in resistivity distribution

$$\Gamma^w_k = E[w_k \cdot w_k^T] \tag{5}$$

Let $U_k \in$ RL, defined as

$$U_k \equiv [U^1_k U^2_k \cdots U^L_k]^T \tag{6}$$

be the surface measurement voltages induced by the kth current pattern. Then the observation equation can be described as the following nonlinear mapping with measurement error

$$U_k = V_k(\rho_k) + v_k \tag{7}$$

where the measurement error vk is also assumed to be white Gaussian noise with covariance

$$\Gamma^v_k = E[v_k \cdot v_k^T] \tag{8}$$

Linearizing (7) about the current predicted state $\rho_{k|k-1}$ we obtain

$$U_k = V_k(\rho_{k|k-1}) + J_k(\rho_{k|k-1}) \cdot (\rho_k - \rho_{k|k-1}) + H.O.T + v_k \tag{9}$$

where H.O.T represents the higher-order terms which will be considered as additional noise, and $J_k(\rho_{k|k-1}) \in R^{L \times N}$ is the Jacobian matrix defined by

$$J_k(\rho_{k|k-1}) \equiv \frac{\partial V_k}{\partial \rho} \Big|_{\rho = \rho_{k|k-1}} \tag{10}$$

Let us define the pseudo-measurement as

$$y_k \equiv U_k - V_k(\rho_{k|k-1}) + J_k(\rho_{k|k-1}) \cdot \rho_{k|k-1} \tag{11}$$

Then we obtain the linearized observation equation by considering the H.O.T in (9) as additional noise

$$y_k = J_k(\rho_{k|k-1}) \cdot \rho_k + \bar{v}_k \tag{12}$$

where $\bar{v}_k$ is composed of measurement error and linearization error and also assumed to be white Gaussian noise with covariance as

$$\bar{\Gamma}_k \equiv E[\bar{v}_k \bar{v}_k^T] \tag{13}$$

k In Kalman filtering we estimate the state ρ_k based on all the measurements taken up to the time k. With the Gaussian assumptions the required estimate is obtained by minimizing the cost functional which is formulated based on the above state and observation equations (4) and (12), respectively. The cost functional for the conventional Kalman filter is of the form

$$G^a(\rho_k) = \frac{1}{2}\{\| \rho_k - \rho_{k|k-1} \|_{C^{-1}_{k|k-1}} + \| y_k - J_k(\rho_{k|k-1}) \cdot \rho_k \|_{(\bar{\Gamma}_k)^{-1}}\} \tag{14}$$

where $C_{k|k-1} \in R^{N \times N}$ is the time-updated error covariance matrix, which is defined by

$$C_{k|k-1} \equiv E[(\rho_k - \rho_{k|k-1})(\rho_k - \rho_{k|k-1})^T] \tag{15}$$

In order to mitigate the inherent ill-conditioned nature of the EIT inverse problem, additional constraint is included in the cost functional

$$G^b(\rho_k) = \frac{1}{2}\{\| \rho_k - \rho_{k|k-1} \|_{C^{-1}_{k|k-1}} + \| y_k - J_k(\rho_{k|k-1})\cdot\rho_k \|_{(\bar{\Gamma}_k)^{-1}} + \alpha \| R^*\rho_k \|\} \quad (16)$$

where α is regularization parameter which is chosen a posteriori, and R* is modified regularization matrix. One popular conventional method for the choice for the regularization matrix R is a difference-type matrix on the basis of the generalized Tikhonov regularization technique[18] by the the smoothness assumptions in resistivity distributions. In this method, the resistivity distribution is parameterized such that

$$\rho = \sum_{n=1}^{N} \rho_n \chi_n \quad (17)$$

where χ_n is the characteristic function of the nth finite element. The ith row of R is

$$R_i = (0,0,...,0,-1,0,...,0,-1,0,...,0,3,0,...,0,-1,0,...0) \quad (18)$$

where 3 is located at the ith column and 1 is placed in the columns corresponding to elements having common edge with the ith element. Sometimes in real situations, there are partially known internal structures in which additional electrodes can be attached. In this case, the modified regularization matrix R^* is obtained from R by removing the 1 in (18) that corresponds to element having common edge with the known internal structure. In that case, the number 3 in (18) is also replaced by 2 since the smoothness assumption is violated between the known element and background.

Define the augmented pseudo-measurement $\bar{y}_k \in R^{(L+N)\times 1}$, and pseudo-measurement matrix, $H_k \in R^{(L+N)\times N}$ as

$$\bar{y}_k \equiv \begin{pmatrix} y_k \\ 0 \end{pmatrix} \quad (19)$$

$$H_k \equiv \begin{pmatrix} J_k \\ \sqrt{\alpha} R^* \end{pmatrix} \quad (20)$$

Then the cost functional, (16) can be rearranged as

$$G(\rho_k) = \frac{1}{2}\{\| \rho_k - \rho_{k|k-1} \|_{C^{-1}_{k|k-1}} + \| \bar{y}_k - H_k\rho_k \|_{(\Gamma_k)^{-1}}\} \quad (21)$$

where the augmented covariance matrix, $\Gamma_k \in R^{(L+N)\times(L+N)}$ is defined by

$$\Gamma_k \equiv \text{Blockdiag}[\bar{\Gamma}_k, I_N] \quad (22)$$

Minimizing the cost functional in (21) and solving for the updates of the associated covariance matrices we obtain the recursive extended Kalman filter algorithm which consists of the following two steps[26, 27]:

(i) Measurement Updating Step (Filtering)

$$G_k = C_{k|k-1}H_k^T[H_kC_{k|k-1}H_k^T + \Gamma_k]^{-1} \quad (23)$$

$$C_{k|k} = (I - G_kH_k)C_{k|k-1} \quad (24)$$

$$\rho_{k|k} = \rho_{k|k-1} + G_k[\bar{y}_k - H_k\cdot\rho_{k|k-1}] \quad (25)$$

(ii) Time Updating Step (Prediction)

$$C_{k+1|k} = F_kC_{k|k}F_k^T + \Gamma_k^w \quad (26)$$

$$\rho_{k+1|k} = F_k\rho_{k|k} \quad (27)$$

Hence, we can find the estimated state $\rho_{k|k}$ for the true state ρ_k in a recursive minimum mean square error sense for k=1,2,...,rK, where K is the number of the independent current patterns and r is the number of the classical frames. As a result, the only difference between the conventional EKF and the proposed EKF which includes a priori information for the partially known internal structure is that the dimension of the measurement updating procedure is increased.

IV. Computer Simulations

We carried out extensive computer simulations with synthetic data to evaluate the reconstruction performance of the proposed algorithm. In the simulations, the complete electrode model with the contact impedance of $0.005\Omega cm(Z_l)$ is employed.

The FEM meshes without internal electrodes used for the forward and inverse solvers are shown in Fig. 1 (a) and (b), respectively. In the forward computations we used the FEM with a mesh of 2400 elements and 1281 nodes (M). In the inverse computations, we used the FEM with a mesh of 600 elements (N) and 341 nodes

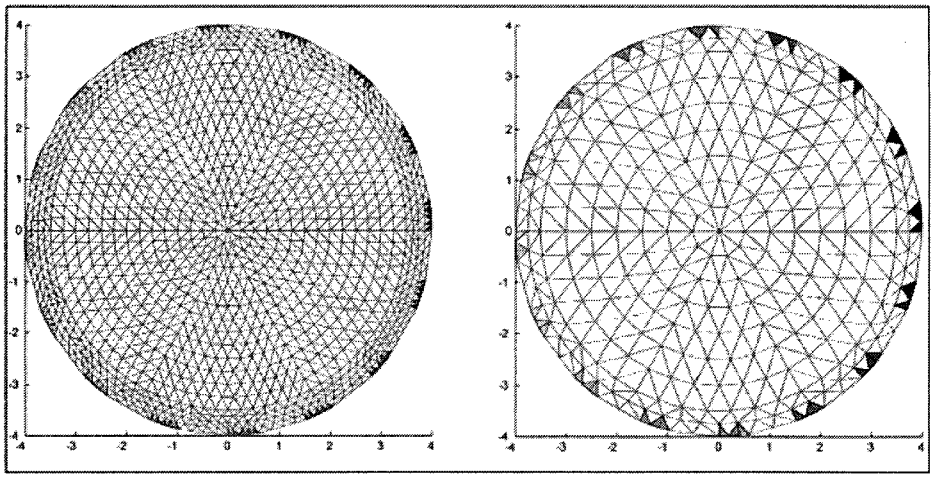

(a) (b)

Fig. 1. FEM meshes without internal electrodes used for (a) forward solver and (b) inverse solver.
그림1. 내부 전극을 사용하지 않은 일반 FEM mesh(a) 정문제 mesh (b) 역문제 mesh

to reduce the computational burden. For the current injection and corresponding voltage measurement, traditional adjacent method[1] was employed through 16 boundary electrodes(L) so that the total measurement voltage data were 256(16×16).

The FEM meshes with 4 internal electrodes used for the forward and inverse solvers are shown in Fig. 2 (a) and (b), respectively. In the forward computations we used the FEM with a mesh of 2544 elements and 1368 nodes (M). In the inverse computations, we used the FEM with a mesh of 636 elements (N) and 366 nodes. We injected electrical current between 16 boundary electrodes and one of the internal electrode and measured the corresponding voltage on the 20

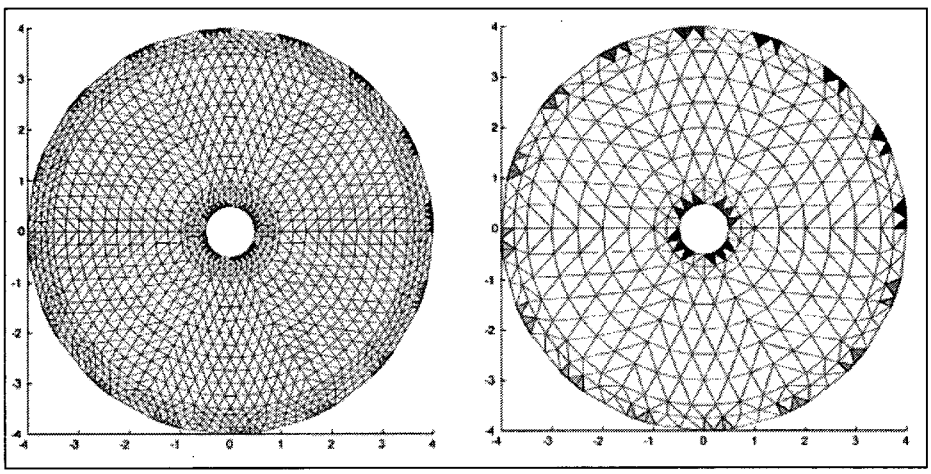

(a) (b)

Fig. 2. FEM meshes with 4 internal electrodes used for (a) forward solver and (b) inverse solver.
그림2. 4개의 내부전극을 사용한 FEM mesh (a) 정문제 mesh (b) 역문제 mesh

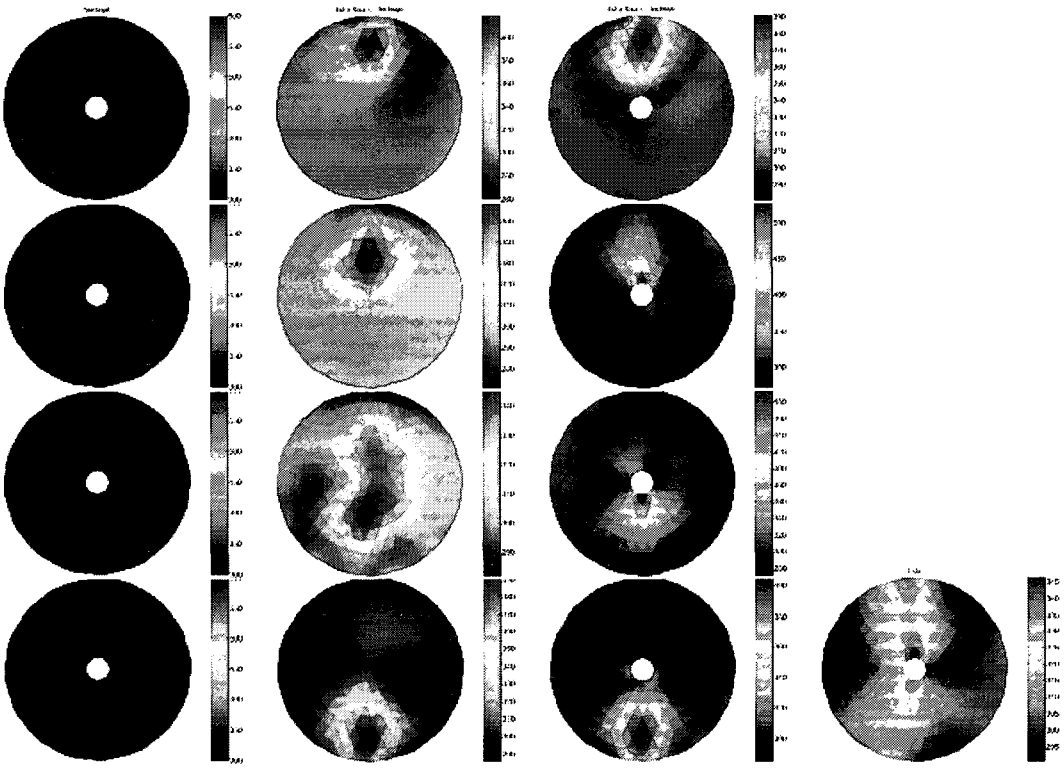

(a) (b) (c) (d)

Fig. 3. Reconstructed images from the first simulation. (a) True target images, (b) reconstructed images by the EKF, (c) reconstructed images by the EKF-IE and (d) reconstructed images by the mNR-IE.
그림3. 복원된 동적 영상 (a) 실제 타겟의 동적영상 (b) EKF에 의해 복원된 영상
(c) EKF-IE에 의해 복원된 영상 (d) mNR-IE에 의해 복원된 영상

electrodes(L) so that the total measurement voltage data were 320(20×16).

To compare the reconstruction performance, we used the static algorithm based on the modified Newton-Raphson algorithm with internal electrodes (mNR-IE)[23], dynamic algorithm based on the extended Kalman Filter (EKF)[18], and the Extended Kalman Filter with internal electrodes (EKF-IE) described in this paper. The parameters used for the three methods are as follows. The regularization parameter α is set to 0.5 in both simulation. The initial resistivity value is set to the same as the background value in all cases. For simplicity, it is assumed that the covariance matrices for all the EKFs are diagonal and time-invariant. The covariance matrix for process noise(Γ_k^w) is 10IN the covariance matrix for measurement noise(Γ_k^v) is 0.0001IL and the initial value for the state error covariance matrix ($C_{1|0}$) is IN in both simulations.

4.1.1 The first simulation

We generated the following sequence of resistivity distributions to simulate a dynamic situation. We assumed that there is known non-conductive circular structure (about 1 cm in diameter) located at the center of the domain, in which four electrodes are attached. An almost circular-type target (resistivity of $600\Omega cm$) was moved abruptly to the opposite site through near

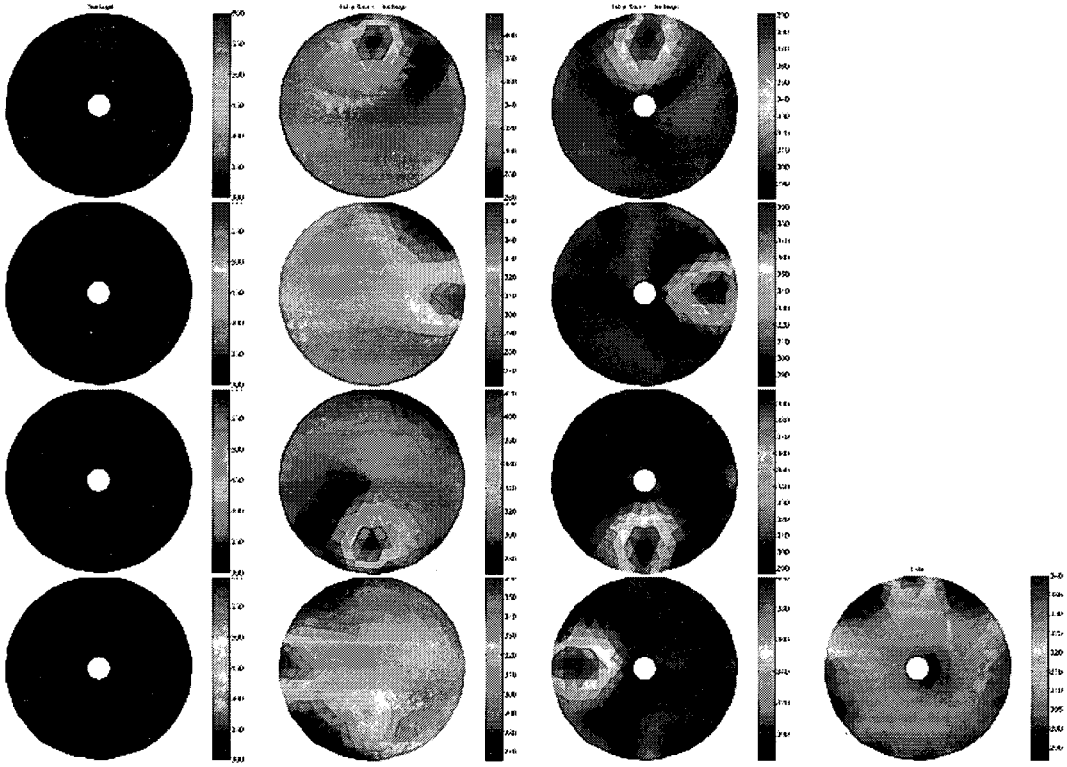

(a) (b) (c) (d)

Fig. 4. Reconstructed images from the second simulation.(a) True target images (b) reconstructed images by the EKF, (c) reconstructed images by the EKF-IE and (d) reconstructed images by the mNR-IE.

그림4. 복원된 동적 영상 (a) 실제 타겟의 동적영상 (b) EKF에 의해 복원된 영상 (c) EKF-IE에 의해 복원된 영상 (d) mNR-IE에 의해 복원된 영상

the center after 4 current patterns in a circular domain(8cm in diameter, $300\Omega cm$ background resistivity) as depicted in the first column of Fig. 3.

Fig. 3 shows the reconstructed images for the three methods. The images in the second column are reconstructed by the EKF without internal electrodes. As can be seen clearly, the location (temporal resolution) of the moving target is rather misleading especially when the target is located near the non-conductive center of the domain(2nd and 3rd rows in the 2nd column). It seems that the error may be generated from the masking effect for the high-contrast. Also, the background was severely blurred by the non-conductive circular structure. The third column represents the reconstructed images from the EKF-IE. As can be expected, the reconstruction performance is improved qualitatively in terms of the temporal and spatial resolution. The reconstructed images obtained from the mNR-IE (fifth column) are also blurred and the information on the time-variability of the moving target is lost since it requires a full set of measurement data.

4.1.2 The second simulation

In the second simulation, we assumed the same scenario for the internal structure as in the first simulation. However, an almost circular-type target (resistivity of $600\Omega cm$) was moved abruptly by 90o clockwise after every 4 current patterns in the same

circular domain as in the first simulation (the first column of Fig. 4).

Figs. 4(b), (c) and (d) represent the reconstructed images obtained by the EKF, EKF-IE and mNR-IE, respectively. As can be seen, the images reconstructed by the EKF without internal electrodes are severely blurred in the homogeneous region (the second column). However, the reconstruction performance of the images obtained by the EKF-IE is enhanced qualitatively(the third column). Also, the temporal information for the abruptly changing targets is severely lost in the reconstructed images by the mNR-IE (the fourth column).

V. Conclusions

Quite often in real situations, there are partially known fixed internal structures inside the object, in which additional internal electrodes could be attached. we have proposed a dynamic EIT reconstruction algorithm for the case where the fixed internal structure are known partially and the resistivity distribution of the other part inside the object changes rapidly within the time taken to acquire a full set of independent measurement data. In doing so, additional internal electrodes are attached to the known internal structures. EIT inverse problem is formulated as a state estimation problem and the state (resistivity distribution) is estimated with the aid of the EKF after the voltage measurements corresponding to each current pattern.

Computer simulation results showed that the proposed method produces qualitatively better reconstruction performance in the sense of the spatial and temporal resolution than do the other existing methods such as conventional EKF and mNR.

Of course, there are many alternatives to the extended Kalman filter used in this paper. For example, linearized Kalman filter can be replaced by the extended Kalman filter to reduce the on-line computational burden. Further research will be carried out to test the reconstruction performance of the proposed technique for more complicated real situations.

VI. Acknowledgment

This work was supported by the Nuclear Academic Research Program of the Ministry of Science and Technology, South Korea.

REFERENCES

[1] J. G. Webster, Electrical Impedance Tomography, Adam Hilger, 1990.

[2] R. A. Williams and M. S. Beck, Process Tomography : Principles, Techniques and Applications, Butterworth-Heinemann, Oxford, 1995.

[3] M. S. Beck and R. A. Williams, Process tomography : a European innovation and its applications, Measurement Science and Technology, Vol. 7, pp. 215-224, 1996.

[4] C. G. Xie, N. Reinecke, M.S. Beck, D. Mewes, and R. A. Williams, "Electrical tomography techniques for process engineering applications," The Chemical Engineering Journal, Vol.56, pp. 127-133, 1995.

[5] M. Cheney, D. Isaacson, and J. C. Newell, Electrical impedance tomography, SIAM Review, Vol. 41, No. 1, pp. 85-101, 1999.

[6] R. W. M. Smith, I. L. Freeston, and B. H. Brown, "A real-time electrical impedance tomography system for clinical use-Design and preliminary results," IEEE Transactions on Biomedical Engineering, Vol. 42, No.2, pp. 133-140, 1995.

[7] S. L. Ceccio and D. L. George, "Review of electrical impedance techniques for the measurement of multiphase flows," Journal of Fluids Engineering, Vol. 118, pp. 391-399, 1996.

[8] A. J. Peyton, Z. Z. Yu, G. Lyon, S. Al-Zeibak, J. Ferreira, J. Velez, F. Linhares, A. R. Borges, H. L. Xiong, N. H. Saunders, and M. S. Beck, An overview of electromagnetic inductance tomography : description of three different systems, Measurement Science Technology, Vol. 7, pp. 261-271, 1996.

[9] C. G. Xie, S. M. Huang, B. S. Hoyle, R. Thorn, C. Lenn, D. Snowden, and M. S. Beck, Electrical capacitance tomography for flow imaging : system model for development of image reconstruction algorithms and design of primary sensors. IEE Proc. G, Vol. 139, No. 1, pp.89-98, 1992.

[10] F. Dickin and M. Wang, Electrical resistance tomography for process tomography, Measurement Science Technology, Vol. 7, pp. 247-260, 1996.

[11] D. C. Barber and B. H. Brown, Applied potential tomography, Journal of Physics E : Scientific Instrumentation, Vol. 17, pp. 723-733, 1984.

[12] T. J. Yorkey, J. G. Webster, and W. J. Tompkins, "Comparing reconstruction algorithms for electrical impedance tomography," IEEE Transactions on Biomedical Engineering, Vol.34, No.11, pp.843-852, 1987.

[13] M. Vauhkonen, P. A. Karjalainen, and J. P. Kaipio, "A Kalman filter approach to track fast impedance changes in electrical impedance tomography," IEEE Transactions on Biomedical Engineering, Vol.45, No.4, pp. 486-493, 1998.

[14] J.P. Kaipio, P.A. Karjalainen, E. Somersalo, and M. Vauhkonen, "State estimation in time-varying electrical impedance tomography," Annals of New York Academy of Sciences, Vol. 873, pp. 430-439, 1999.

[15] P.J. Vauhkonen, M. Vauhkonen, T.Mäkinen, P.A. Karjalainen, and J.P. Kaipio, "Dynamic electrical impedance tomography Phantom studies, " Inverse Problems in Engineering, Vol. 8, pp. 495-510, 2000.

[16] M. Vauhkonen, "Electrical Impedance Tomography and Prior Information," Doctoral Dissertation, Dept. of Applied Physics, University Kuopio, 1997.

[17] A. Seppanen, M. Vauhkonen, P. J. Vauhkonen, E.Somersalo, and J. P. kaipio, State estimation with fluid dynamical evolution models in process tomography-EIT applications, Inverse Problems, Vol. 17, pp.467-484, 2001.

[18] K. Y. Kim, B. S. Kim, M. C. Kim and Y. J. Lee, On-line image reconstruction in dynamic electrical impedance tomography based on the extended Kalman filter, Proc. of Compumag-Evian (France), Vol. IV, pp. 70-71, 2001.

[19] K. Y. Kim, B. S. Kim, M. C. Kim, Y. J. Lee, and M. Vauhkonen, Image reconstruction in time-varying electrical impedance tomography based on the extended Kalman filter, Measurement Science and Technology, Vol. 12, No. 8, pp. 1032-1039, 2001.

[20] R. A. Williams, X. Jia, and S. L. McKee, Development of slurry mixing models using resistance tomography, Powder Technology, Vo. 87, pp. 21-27, 1996.

[21] L. M. Heikkinen, M. Vauhkonen, T. Savolainen, K. Leinonen, and J. P. Kaipio, "Electrical Process Tomography with known internal structures and resistivities", Inverse Problems in Engineering, 2000 (in press).

[22] G. M. Lyon and J. P. Oakley, A simulation study of sensitivity in stirred vessel electrical impedance tomography, In M. S. Beck, E. Campogrande, M. Morris, R. A. Williams, and R. C. Waterfall, editors, Tomography Techniques for Process Design and Operation, pp. 137-146, Southampton UK, 1993, Computational Mechanics Publications.

[23] L. M. Heikkinen, M. Vauhkonen, T. Savolainen, and J. P. Kaipio, Modeling of internal structures and electrodes in electrical process tomography, Measurement Science and Technology, Vol. 12, No. 8, pp. 1012-1019, 2001.

[24] K.S. Cheng, D. Isaacson, J.C. Newell and D.G. Gisser, "Electrode Models for electric current computed tomography, " IEEE Transactions on Biomedical Engineering, Vol. 36, pp.918-924, 1989.

[25] M. Vauhkonen, W.R.B. Lionheart, L.M. Heikkinen, P.J. Vauhkonen and J.P. Kaipio, "A MATLAB package for the EIDORS Project to reconstruct two-dimensional EIT images, " Physiological Measurements, in press.

[26] A. Gelb, Applied Optimal Estimation, The M. I. T. Press, Cambridge, Massachusetts, 1974.

[27] M. S. Grewal and A. P. Andrews, Kalman Filtering : Theory and Practice, Prentice Hall, Englewood Cliffs, New Jersey, 1993.

저 자 소 개

姜 淑 仁

2000년 2월 제주대학교 전자공학과(공학사)
2001년 - 현재 제주대학교 전자공학과 석사과정
<주관심분야> Electrical tomography, Kalman 필터 응용 등

金 慶 淵

1983년 2월 경북대학교 전자공학과(공학사)
1986년 2월 경북대학교 전자공학과(공학석사)
1990년 2월 경북대학교 전자공학과(공학박사)
1994년 - 1995년 Univ. of Maryland(Postdoc)
1990년 3월 - 현재 제주대학교 전기전자공학부(전임강사/조교수/부교수/교수)
<주관심분야> Target tracking, Fault detection and diagnosis, Electrical tomography 등